

Effect of dislocation structure evolution on low-angle grain boundary formation in 7050 aluminum alloy during aging

Wei Gu, Jing-yuan Li, and Yi-de Wang

School of Materials Science and Engineering, University of Science and Technology Beijing, Beijing 100083, China
(Received: 6 January 2015; revised: 19 March 2015; accepted: 24 March 2015)

Abstract: The effect of dislocation structure evolution on low-angle grain boundary formation in 7050 aluminum alloy during aging was studied by using optical microscopy, transmission electron microscopy, and electron backscatter diffraction analysis of misorientation angle distribution, cumulative misorientation and geometrically necessary dislocation (GND) density. Experimental results indicate that coarse spindle-shaped grains with the dimension of $200\ \mu\text{m} \times 80\ \mu\text{m}$ separate into fine equiaxed grains of $20\ \mu\text{m}$ in size as a result of newborn low-angle grain boundaries formed during the aging process. More specifically, the dislocation arrays, which are rearranged and formed due to scattered dislocations during earlier quenching, transform into low-angle grain boundaries with aging time. The relative frequency of 3° – 5° low-angle grain boundaries increases to over 30%. The GND density, which describes low-angle grain boundaries with the misorientation angle under 3° , tends to decrease during initial aging. The inhomogeneous distribution of GNDs is affected by grain orientation. A decrease in GND density mainly occurs from 1.83×10^{13} to $4.40 \times 10^{11}\ \text{m}^{-2}$ in grains with $\langle 111 \rangle$ fiber texture. This is consistent with a decrease of unit cumulative misorientation. Precipitation on grain boundaries and the formation of a precipitation free zone (PFZ) are facilitated due to the eroding activity of the Graff etchant. Consequently, low-angle grain boundaries could be readily viewed by optical microscopy due to an increase in their electric potential difference.

Keywords: aluminum alloys; low-angle grain boundaries; dislocation structure; aging; dislocation density

1. Introduction

Grain boundaries in a polycrystalline aluminum alloy have both beneficial as well as detrimental effects on the properties of the alloy. For example, the presence of grain boundaries strengthens the alloy by hindering the gliding of dislocations in grains, while it deteriorates the corrosion properties due to increasing electric potential difference between the matrix and the boundaries. Therefore, the evolution of grain boundaries is of great importance and has attracted considerable interest among researchers. In general, a low-angle grain boundary (LAGB) is modeled to be composed of an array of parallel dislocations and separates regions of different crystallographic orientations. Besides, dislocations in a crystal could be classified into two categories, namely, geometrically necessary dislocations (GNDs), which contribute to the curvature of the crystal lattice, and statistically stored dislocations (SSDs), which evolve

through random interactions among dislocations during plastic deformation. Therefore, LAGB evolution includes the following processes, namely, GND tangling, annihilation, and rearrangement.

In general, LAGBs are produced via gliding, tangling, and rearrangement of dislocations in grains during plastic deformation [1]. Till date, several studies have focused on using GND as a feasible method to establish a relationship between plastic deformation and dislocations [2–5]. For instance, Ruggles and Fullwood [2] measured the density of GNDs using local crystal orientation by integrating high-resolution electron backscatter diffraction (EBSD) beneath the indenters. As demonstrated in the Taylor model, the number of activated slip systems differs significantly for various grain orientations of polycrystalline materials under plastic deformation. Merriman *et al.* [3] have determined the largest GND density occurring in grains with $\{011\}[122]$ orientation after plane strain deformation. Based on LAGB

Corresponding author: Jing-yuan Li E-mail: lijy@ustb.edu.cn

© University of Science and Technology Beijing and Springer-Verlag Berlin Heidelberg 2015

model, Zhu and Xiang [4] have presented a continuum framework to define the dislocation density potential function on the dislocation array and LAGB. Furthermore, Winther *et al.* [5] have studied the relationship between crystallographic orientation of planar dislocation boundaries and grain orientation under tension. Quey *et al.* [6] studied microtexture tracking of sub-boundary evolution during hot deformation of aluminum.

In principle, residual stress relaxation generated by dislocations is a driving force for grain recovery to form LAGBs [7–9]. Wang *et al.* [10] reported that residual stress relaxation caused by a vibratory stress relief technique results in a decrease in dislocation density and formation of LAGBs. However, in the metal forming industry, heat treatment is a more widespread stress relief method. In particular, it is essential for strengthening the alloy during aging, together with the advantage of relaxing the residual stress. Nevertheless, the lack of studies on LAGB evolution during aging has led to a greater deviation of aging strengthening because of grain refinement and precipitation on LAGB [11–12].

Lately, there has been rapid development in automated EBSD techniques in terms of indexing speed and accuracy [2,13–15]. More importantly, the EBSD technique is combined with the continuum dislocation theory to establish GND density calculation [16–17], which fills the scale gap of microstructure observation between EBSD and transmission electron microscopy (TEM). The purpose of the present study is to analyze LAGB evolution during aging and determine the inhomogeneous distribution of GND density acquired by this calculation in grains with three different types of fiber texture during initial aging. Further studies are underway to analyze the effect of grain boundary strengthening mechanics and precipitation on LAGBs.

2. Experimental

2.1. Materials

Commercial 7050 aluminum alloy used in this study was obtained via hot extrusion thick profiles. The chemical composition of the alloy is shown in Table 1.

Table 1. Chemical composition of the investigated 7050 aluminum alloy

							wt%
Zn	Mg	Cu	Zr	Fe	Si	Ti	Al
5.84	2.32	2.04	0.11	0.039	0.041	0.012	Bal.

In order to ensure homogeneous composition and identical grain structures, specimens were cut out from the center

of the heaviest section in the extrusion profiles by wire electrical discharge. Subsequently, the specimens were solution treated at 477°C for 1 h to obtain a relatively dislocation-free microstructure, followed by rapid quenching in water at ambient temperature with the transferring time from the heating furnace to water being less than 3 s. This thermal gradient caused by the sudden quenching induces residual stresses in the specimen [18–19]. Details on the heat treatment procedures of these specimens are listed in Table 2.

Table 2. Description of heat treatment procedures adopted for the 7050 Al alloy in this study

Sample name	Solution treatment
SQ	(477°C, 1 h) + Quenching
A121-30	(477°C, 1 h) + Quenching + (121°C, 30 min)
A121-360	(477°C, 1 h) + Quenching + (121°C, 360 min)
A177-5	(477°C, 1 h) + Quenching + (121°C, 360 min) + (177°C, 5 min)
A177-60	(477°C, 1 h) + Quenching + (121°C, 360 min) + (177°C, 60 min)

2.2. Microstructure characterization

The surfaces perpendicular to the extruding direction of the specimens were mechanically ground and polished. After etching with Graff [20] solution and Keller solution, the microstructure of the specimens was observed using an optical microscope (OM, Leica DM2500M).

Thin foils for TEM observation were prepared by twinjet electro-polishing in a solution of 30vol% nitric acid in methanol at –30°C and 12 V. The bright-field TEM images of the specimens were obtained by using TEM (JEM-2010 JEDL) operated at 200 kV, in order to observe the dislocations, sub-grain boundaries, and precipitation on the grain boundaries.

After mechanical polishing, the specimens were subsequently electro-polished in 15vol% nitric acid methanol solution at –20°C and 15 V. The grain orientation was identified using the EBSD technique equipped with a LEO-1450 scanning electron probe. The EBSD analysis yielded orientation imaging microscopy (OIM) maps, misorientation angle distribution (MAD), and line misorientation (LM). The LAGBs were composed of low disoriented LAGBs (LLAGBs, < 3°), medium disoriented LAGBs (MLAGBs, 3°–5°), and high disoriented LAGBs (HLAGBs, 5°–15°). The high-angle grain boundaries (HAGB) are defined as the grain boundaries with misorientation angle greater than 15°.

2.3. Calculation of GND density

Previous studies have proven that the selection of scan-

ning step size is a key parameter for accurate calculation of GND density [15,21]. Therefore, scanning with a higher scan step size of 3 μm was performed to statistically obtain the fiber texture of the polycrystalline material. Similarly, another scanning with a smaller scan step size of 0.5 μm was performed to collect information on local orientation for point-to-point misorientation within grains, which met the precision need for GND density calculation. All number averages are translated directly to averages of the grain area owing to the principle of DeLesse.

The GND density was calculated and illustrated in figures by independently programming in the MATLAB software using the original local orientation data of EBSD [17,22–24]. In the GND density maps, the black region represents higher dislocation density. The geometrical independence of dislocations and slip systems was fully considered during the programming process.

3. Results and discussion

3.1. Optical microscopy analysis

Figs. 1(a)–1(f) show the OM images of 7050 aluminum alloy obtained through five heat treatment procedures. The specimens etched using Graff solution are shown in Figs. 1(a)–1(e), while the specimen etched using Keller solution is shown in Fig. 1(f). Specimens shown in Figs. 1(e) and 1(f) are processed under identical aging conditions. The recovery and recrystallization processes have occurred during the solution treatment stage. As can be seen from the OM image shown in Fig. 1(a), the fiber grains present a spindle-like morphology, with a long axis length of about 200 μm and the short axis length of about 80 μm , under the influence of extrusion. The grain size and morphology do not change significantly during the initial stages of aging (Figs. 1(b)–1(c)). However, more unclosed grain boundaries could

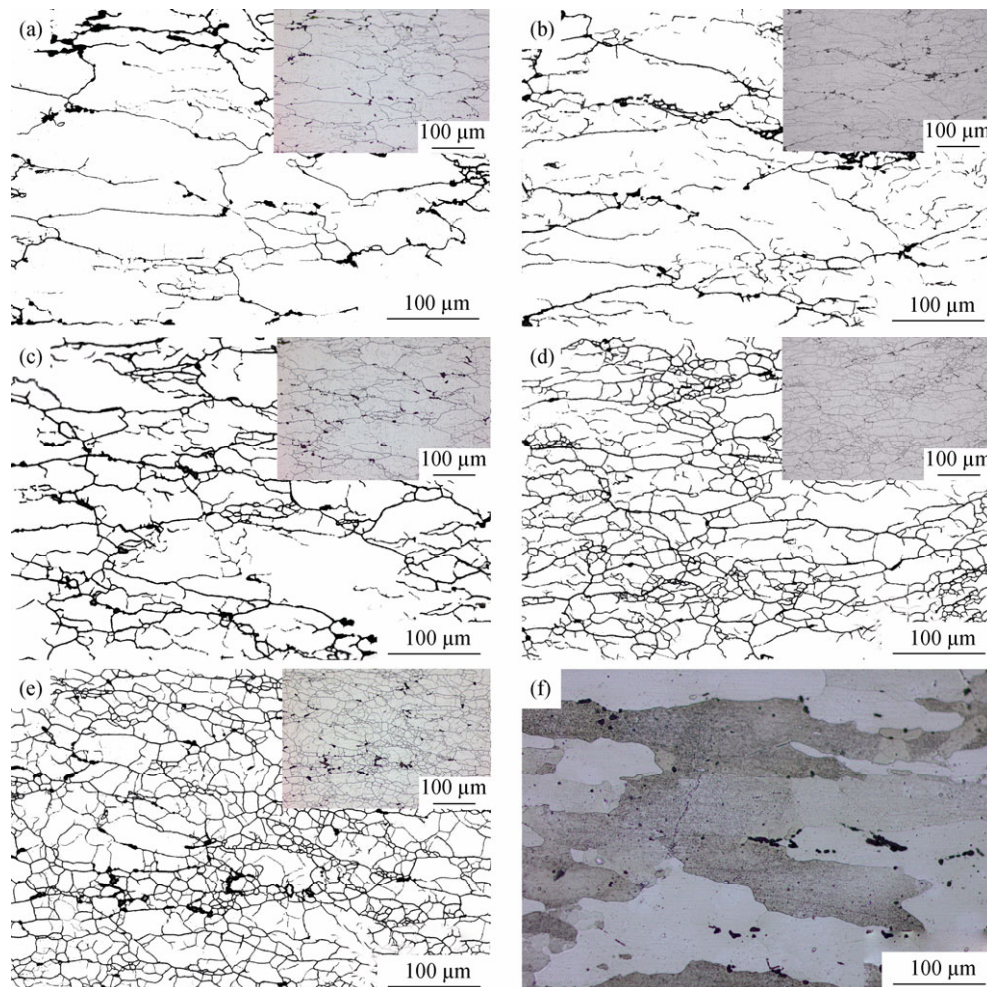


Fig. 1. Grain boundary skeletons extracted from optical micrographs of the specimens, which are shown on the upper-right corner of the images. These specimens were obtained through five different heat treatment processes: (a) SQ; (b) A121-30; (c) A121-360; (d) A177-5; (e) and (f) A177-60. All specimens were etched using Graff etchant, except the specimen in (f) which was etched using Keller etchant.

be observed in the grains of A177-5 specimen, as shown in Fig. 1(d). With an increase in the unclosed grain boundaries, the former coarse spindle-shaped grains are further broken into fine equiaxed grains of dimension 20 μm , as shown in Fig. 1(e). Compared with the microstructure shown in Fig. 1(e), the microstructure of the A177-60 specimen etched using Keller etchant (as seen in Fig. 1(f)) does not reveal any subgrain boundaries. Or in other words, the microstructure was similar to the structure shown in Fig. 1(a). These results demonstrate that the newborn grain boundaries within the coarse grains are LAGB and that they can only be viewed using Graff etchant.

3.2. TEM analysis

Figs. 2(a)–2(d) show the TEM bright-field images of the specimens SQ, A121-30, A121-360, and A177-5, respectively. The 7050 aluminum alloys contain several alloy

elements that tend to increase the dislocations upon quenching after the treatment at 477°C [25]. As seen in Fig. 2(a), the dislocations are scattered in the grains, which curve the crystallographic lattice plane and store elastic strain energy in the SQ specimen. This sub-structure is rather unstable and hence tends to release the elastic strain energy. Therefore, the dislocations are rearranged upon initial aging at 121°C, as shown in Fig. 2(b). Dislocation arrays are formed as a result of scattered dislocations, some of which integrate into LAGB at 121°C for longer time, as depicted in Fig. 2(c). However, the integration of dislocation arrays and the migration of LAGBs after aging at 177°C for 5 min are hindered due to the precipitation occurring in grains, as shown in Fig. 2(d). Meanwhile, the precipitation free zone (PFZ) is formed and the eroding ability of LAGBs is enhanced by Graff to be viewed in OM.

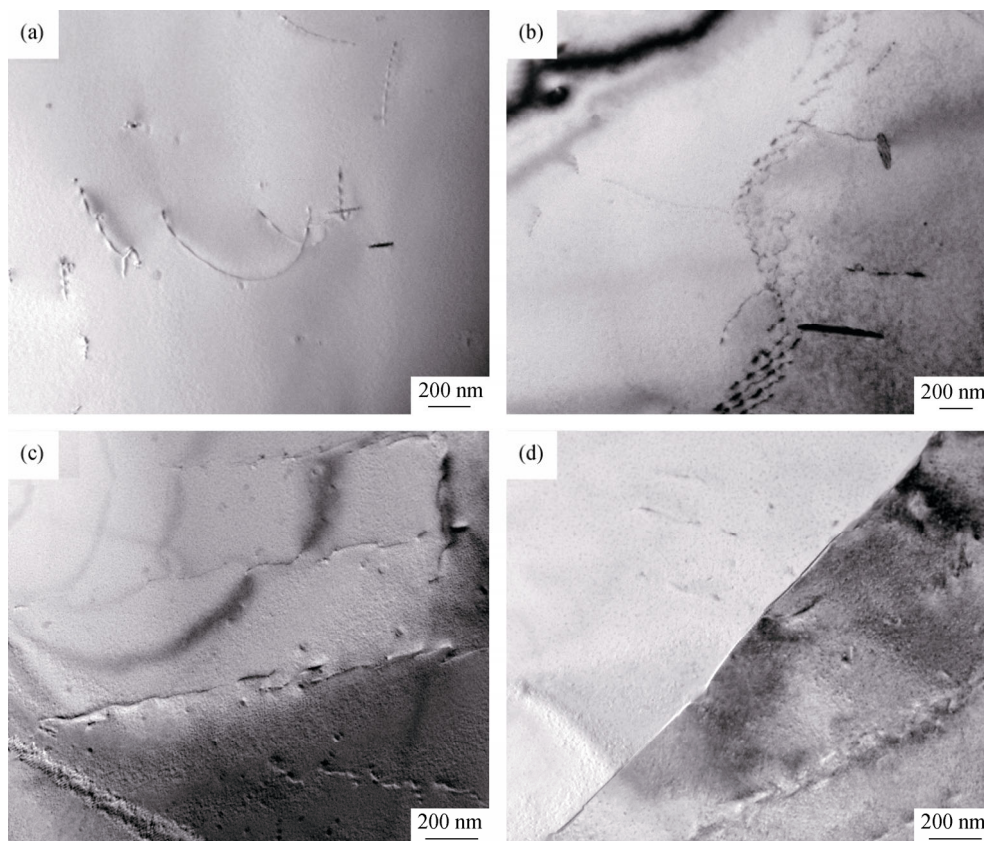


Fig. 2. TEM images showing the scattered dislocations, dislocation arrays, and LAGBs in 7050 Al alloy specimens treated by solid solution (a), aging at 121°C for 30 min (b), aging at 121°C for 360 min (c), and aging at 177°C for 5 min (d).

3.3. EBSD analysis

Fig. 3 shows the misorientation angle distribution of grain boundaries in specimens obtained by various heat treatments. Except for LLAGBs, the evolution of MLAGBs

can also be observed. It seems that the relative frequency of MLAGBs accounts for over 30% of LAGBs in Fig. 3. Moreover, the relative frequency of MLAGBs shows a downward trend after an initial increase. Besides, the LAGBs in aged specimens exhibit higher volume fraction

than that in as-quenched specimen. Among all aged specimens the A121-360 has the highest volume fraction of LAGBs. This could be explained by the formation of LAGBs, which is due to the integration of scattered dislocations, as depicted in Fig. 2(c). Heat from the initial aging to the secondary aging thermally facilitates the integration of LLAGBs. Herein, little precipitation occurs due to the misorientation angle less than 3° [26], while there is a reduction in the volume fraction of MLAGBs. In addition, the

precipitation, which favors nucleation on MLAGBs and HLAGBs during aging, hinders the transformation from LAGBs to HAGBs.

Figs. 4(a)–4(e) illustrate the color depiction of the distribution of four fiber textures, i.e., <100> texture, <110> texture, <111> texture, and other random texture within various specimens. The relative frequency of these fiber orientations stays stable with aging owing to the solution alloy elements, i.e., magnesium [1].

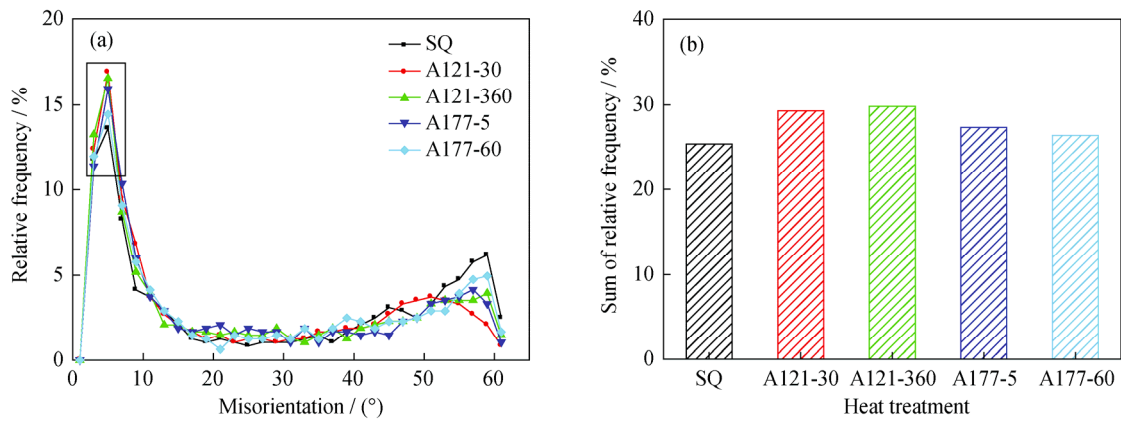


Fig. 3. (a) Relative frequency of the misorientation angles of GBs and (b) sum of relative frequency of MLAGBs marked by the black rectangle block in Fig. 3(a) after five heat treatments.

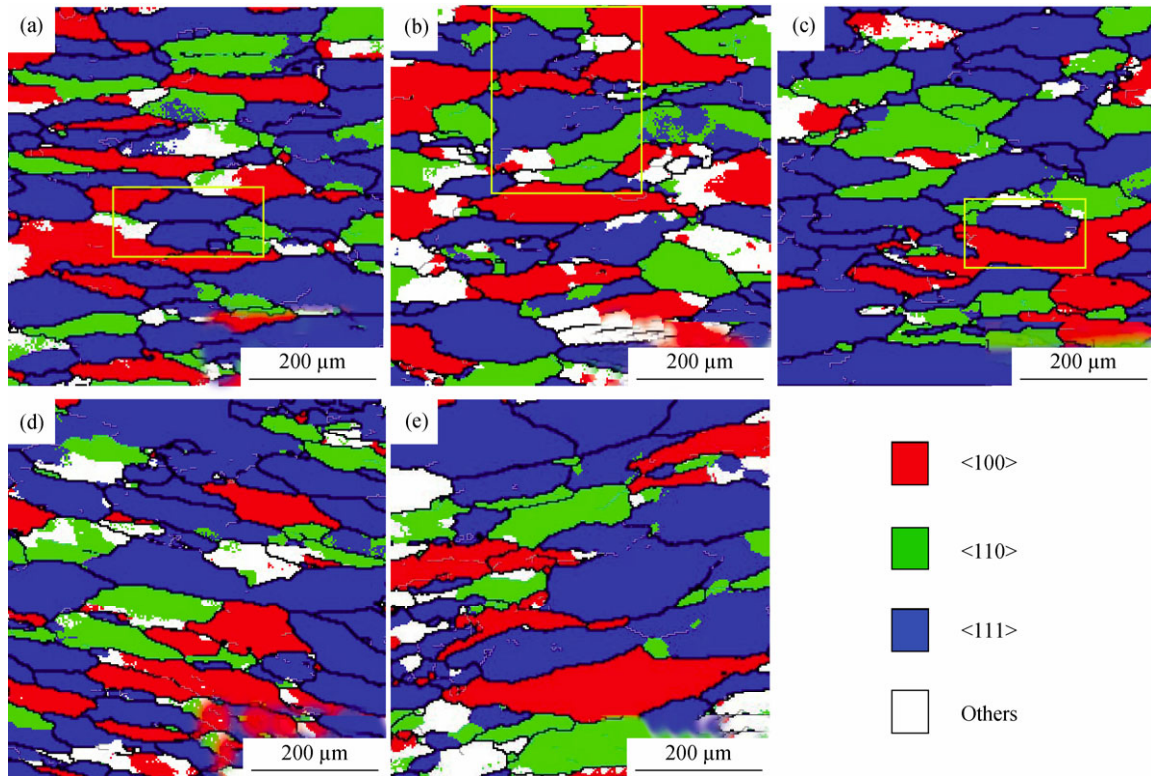


Fig. 4. EBSD orientation maps showing the fiber textures of SQ (a), A121-30 (b), A121-360 (c), A177-5 (d), and A177-60 (e). Grains with <100>, <110>, <111>, and other fiber textures are illustrated using different colors. Geometrically necessary dislocations were calculated in the region marked by yellow line frames.

Fig. 5 demonstrates the unit cumulative misorientation ($\Delta\theta_1/l_1$) in the grains of SQ, A121-30, and A121-360 specimens. The line scan of misorientation measurement never crosses any grain boundaries along the long axis of the grains. The value of $\Delta\theta_1/l_1$ represents the average lattice curvature due to residual stress. As shown in Fig. 5, the value of $\Delta\theta_1/l_1$ in the $\langle 111 \rangle$ grains has the largest decrease during initial aging, while that in the $\langle 110 \rangle$ grains has the smallest change.

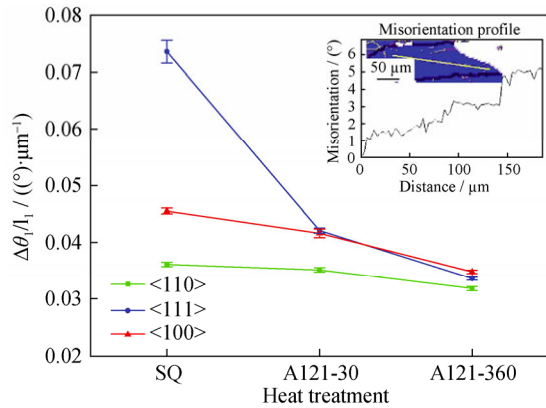


Fig. 5. Variation of unit cumulative misorientation ($\Delta\theta_1/l_1$) with the first aging time of the solid-solution treated specimen. As shown in the upper-right corner of this figure, $\Delta\theta_1/l_1$ is statistically calculated as cumulative misorientation (point-to-origin) as a function of distance, and from one grain boundary to another in grains. Note that the line is nearly parallel to the long axis of the grain and does not cross any grain boundaries.

3.4. GND density calculation

Furthermore, we calculated the GNDs in order to analyze the evolution of its density on different fiber textures and its effect on the formation of LLAGB in grains during the ini-

tial stages of aging, as seen in Fig. 6. The regions enclosed in yellow line frames in Fig. 4 correspond to the regions for which the density of GNDs is calculated. The small white bands around black line, shown in Fig. 6, represent HAGBs or the regions poorly indexed in EBSD. Conversely, gray scale corresponds to black regions with GND density more than $8.5 \times 10^{13} \text{ m}^{-2}$ to white regions with GND density less than $1.5 \times 10^{12} \text{ m}^{-2}$. The GND density presents homogeneous distributions in grains with different crystallographic orientations of the SQ specimen (Fig. 6(a)). As shown in Fig. 6(b), the GND density distributions are not homogeneous; rather, they are in the form of dislocation arrays within the grain. However, as demonstrated in Fig. 2, the dislocations glide, aggregate, and rearrange within the grains of A121-30 and A121-360 (Figs. 6(b)–6(c)). Dislocation arrays and LLAGBs are formed and consist of GNDs. Therefore, the volume fraction of MLAGBs increases during the initial aging processes, as seen in Fig. 3.

Fig. 7(a) shows a continual decrease in the sum of GND density, with the specimen A121-360 having the lowest GNDs density. The inhomogeneous distribution of GND density in grain orientation becomes more apparent in Fig. 7(b). Owing to the gathering and collapsing of several dislocations into LLAGBs, there is a decrease in the volume fraction of GND density to a lower level [27]. Besides, the GND density of the regions around LLAGBs is smaller in grains, as seen in Figs. 6(a)–6(c). Fig. 7(b) shows the statistical distribution of average GND density in grains with $\langle 111 \rangle$, $\langle 110 \rangle$, and $\langle 100 \rangle$ fiber textures in A121-30. The most consumption of GNDs from $1.83 \times 10^{13} \text{ m}^{-2}$ to $4.40 \times 10^{11} \text{ m}^{-2}$ occurs in $\langle 111 \rangle$ grains. This consumption causes the LLAGBs to form and disorient, which leads to the highest density of MLAGBs and the lowest one of LLAGBs in $\langle 111 \rangle$ grains among the three fiber grains.

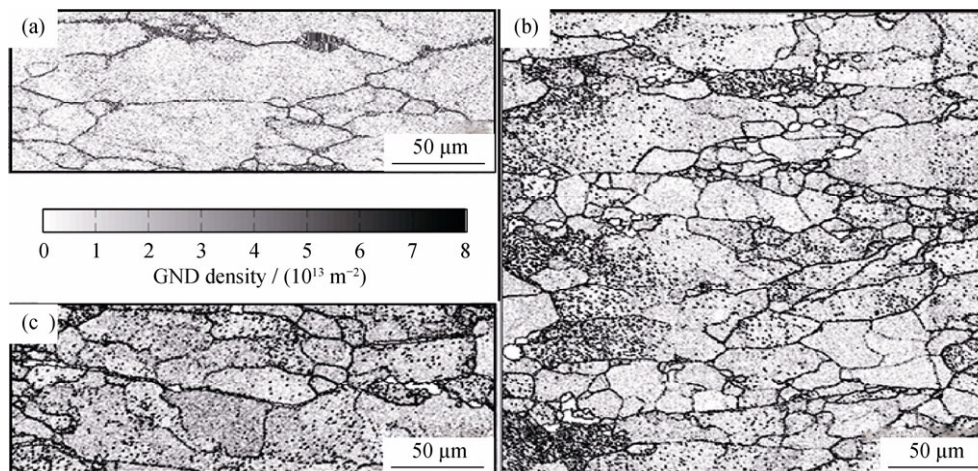


Fig. 6. GND density maps for orientation images in the region marked by yellow line frames in Fig. 4, which represent the GND content of the specimen SQ (a), A121-30 (b), and A121-360 (c).

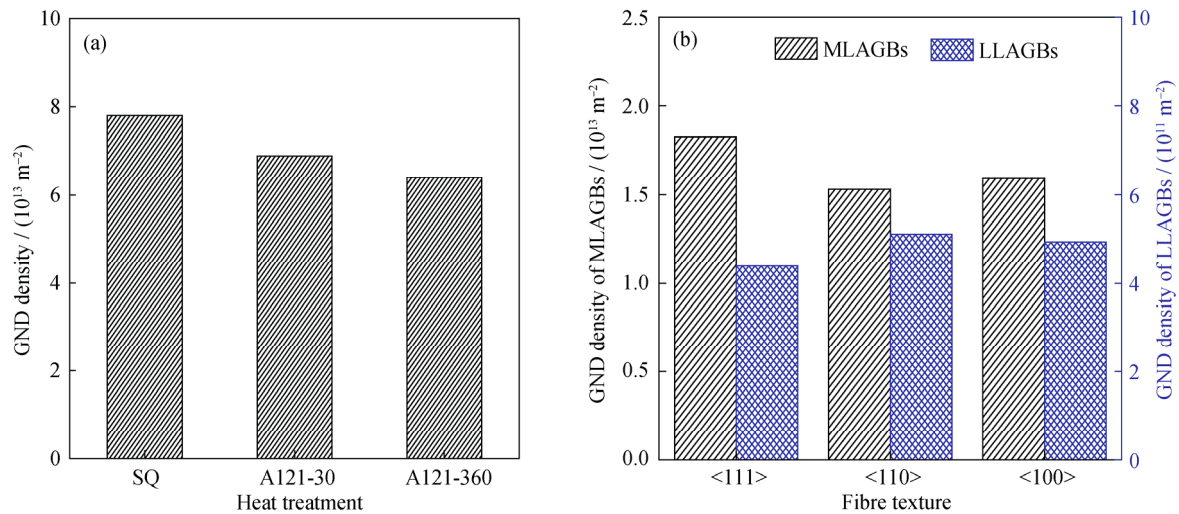


Fig. 7. (a) Histograms showing the total GND density in specimens and (b) GND density of MLAGBs and LLAGBs in different fiber texture grains.

3.5. Mechanism underlying LAGB formation by GND

Heat during the initial stages of aging plays a critical role in relaxing quenching residual stress. As shown in Fig. 2, the quenching dislocations are rearranged into a dislocation array, the gliding of which will lower the system energy and stabilize the sub-structure. During the initial stages of aging, the decrease of GND density has a contrast with increase in the fraction of the MLAGBs, as shown in Figs. 6 and 3.

During aging, 7050 aluminum alloys are not subject to external stress. Therefore, the stress components are not formed due to crystal stress anisotropy as demonstrated in the Taylor model. The Taylor factor could not be calculated, given the fact that the quenching residual stress does not have a straightforward direction, but a macroscopic homogeneous distribution. However, the GND density in various grains, including <100>, <110>, and <111>, can indirectly reflect the stress to some extent. Ultimately, the harder grain with the highest GND density would activate more slip systems [3]. The dislocations activated by heat may glide along the lowest energy barrier. As the crystal structure of 7050 aluminum alloy is a face-centered-cubic structure, the primary slip system is $\{111\}\langle 110 \rangle$ and the secondary slip system is $\{110\}\langle 111 \rangle$ [17]. It demonstrates that the slip systems activate firstly in <111> grains, followed readily by the gliding of dislocations. The cumulative misorientation has the most precipitous decrease in grains with <111> fiber texture. As shown in Fig. 6(b), most GND density aggregates into grain with <111> fiber texture, upon holding for 30 min at 121°C. As aging proceeds, the dislocation tends to slip and climb up into an array, contributing to an increasingly well-defined sub-structure in the grains. Subsequently, the lattice curvature reduces, thereby releasing the residual stress.

4. Conclusion

It is beneficial to form dislocation arrays via the aggregation of GNDs in grains, which lower the GND density during initial aging. Dislocation arrays are merged and transformed into LAGBs as a result of the aging process. The MLAGBs account for over 30% of LAGBs and show a downward trend after the initial decrease. This could be attributed to the integration of LLAGBs during the aging process, resulting in a decrease in cumulative misorientation and residual stress relaxation. The GND density has an inhomogeneous distribution, showing a significant variation from $1.83 \times 10^{13} \text{ m}^{-2}$ to $4.40 \times 10^{11} \text{ m}^{-2}$, in grains with <111> fiber texture due to the most activated slip system. The precipitation on grain boundaries and the formation of PFZ facilitate the eroding of the specimen surface by Graff etchant, which will allow us to view the LAGBs due to an increase in the electric potential difference.

References

- [1] F.J. Humphreys and M. Hatherly, The structure and energy of grain boundaries, [in] *Recrystallization and Related Annealing Phenomena*, 2nd Ed., Edited by F.J.H. Hatherly, Elsevier, Oxford, 2004, p. 91.
- [2] T.J. Ruggles and D.T. Fullwood, Estimations of bulk geometrically necessary dislocation density using high resolution EBSD, *Ultramicroscopy*, 133(2013), p. 8.
- [3] C.C. Merriman, D.P. Field, and P. Trivedi, Orientation dependence of dislocation structure evolution during cold rolling of aluminum, *Mater. Sci. Eng. A*, 494(2008), No. 1-2, p. 28.
- [4] X.H. Zhu and Y. Xiang, Continuum framework for disloca-

- tion structure, energy and dynamics of dislocation arrays and low angle grain boundaries, *J. Mech. Phys. Solids*, 69(2014), p. 175.
- [5] G. Winther, X. Huang, and N. Hansen, Crystallographic and macroscopic orientation of planar dislocation boundaries: correlation with grain orientation, *Acta Mater.*, 48(2000), No. 9, p. 2187.
- [6] R. Quey and J.H. Driver, Microtexture tracking of sub-boundary evolution during hot deformation of aluminium, *Mater. Charact.*, 62(2011), No. 12, p. 1222.
- [7] A. Baczmański, N. Hfaiedh, M. François, and K. Wierzbowski, Plastic incompatibility stresses and stored elastic energy in plastically deformed copper, *Mater. Sci. Eng. A*, 501(2009), No. 1-2, p. 153.
- [8] K.S. Havner, C. Singh, and R. Varadarajan, Plastic deformation and latent strain energy in a polycrystalline aluminum model, *Int. J. Solids Struct.*, 10(1974), No. 8, p. 853.
- [9] A. Baczmański, K. Wierzbowski, A. Benmarouane, A. Lodini, P. Lipinski, and B. Bacroix, Stored energy and recrystallization process, *Mater. Sci. Forum*, 539-543(2007), p. 3335.
- [10] J.S. Wang, C.C. Hsieh, C.M. Lin, E.C. Chen, C.W. Kuo, and W.T. Wu, The effect of residual stress relaxation by the vibratory stress relief technique on the textures of grains in AA 6061 aluminum alloy, *Mater. Sci. Eng. A*, 605(2014), p. 98. M
- [11] P.B. Hirsch, J. Silcox, R.E. Smallman, and K.H. Westmacott, Dislocation loops in quenched aluminium, *Philos. Mag.*, 3(1958), No. 32, p. 897.
- [12] W. Gu, J.Y. Li, Y.D. Wang, J.Y. Lu, and Y.H. Zhou, Effect of quenching elastic strain energy on evolution of sub-grain boundaries in 7050 Al alloy during aging, *Chin. J. Nonferrous Met.*, 24(2014), No. 9, p. 2257.
- [13] D. Dingley, Progressive steps in the development of electron backscatter diffraction and orientation imaging microscopy, *J. Microsc.*, 213(2004), No. 3, p. 214.
- [14] D.P. Field, P.B. Trivedi, S.I. Wright, and M. Kumar, Analysis of local orientation gradients in deformed single crystals, *Ultramicroscopy*, 103(2005), No. 1, p. 33.
- [15] J. Jiang, T.B. Britton, and A.J. Wilkinson, Measurement of geometrically necessary dislocation density with high resolution electron backscatter diffraction: effects of detector binning and step size, *Ultramicroscopy*, 125(2013), p. 1.
- [16] J.F. Nye, Some geometrical relations in dislocated crystals, *Acta Metall.*, 1(1953), No. 2, p. 153.
- [17] E. Demir, D. Raabe, N. Zaafarani, and S. Zaeferrer, Investigation of the indentation size effect through the measurement of the geometrically necessary dislocations beneath small indenters of different depths using EBSD tomography, *Acta Mater.*, 57(2009), No. 2, p. 559.
- [18] D.A. Tanner and J.S. Robinson, Residual stress prediction and determination in 7010 aluminum alloy forgings, *Exp. Mech.*, 40(2000), No. 1, p. 75.
- [19] D.J. Sharman, H.L. Stark, and D.W. Kelly, Quenching residual stresses in 7060 aluminium alloy gas cylinder necks, *Int. J. Pressure Vessels Piping*, 72(1997), No. 3, p. 193.
- [20] W.R. Graff and D.C. Sargent, A new grain-boundary etchant for aluminum alloys, *Metallography*, 14(1981), No. 1, p. 69.
- [21] L.P. Kubin and A. Mortensen, Geometrically necessary dislocations and strain-gradient plasticity: a few critical issues, *Scripta Mater.*, 48(2003), No. 2, p. 119.
- [22] W. Pantleon, Resolving the geometrically necessary dislocation content by conventional electron backscattering diffraction, *Scripta Mater.*, 58(2008), No. 11, p. 994.
- [23] S. Sun, B.L. Adams, and W.E. King, Observations of lattice curvature near the interface of a deformed aluminium bicrystal, *Philos. Mag. A*, 80(2000), No. 1, p. 9.
- [24] W. Pantleon, W. He, T.O. Johansson, and C. Gundlach, Orientation inhomogeneities within individual grains in cold-rolled aluminium resolved by electron backscatter diffraction, *Mater. Sci. Eng. A*, 483-484(2008), p. 668.
- [25] R.M.J. Cotterill and R.L. Segall, The effect of quenching history, quenching temperature and trace impurities on vacancy clusters in aluminium and gold, *Philos. Mag.*, 8(1963), No. 91, p. 1105.
- [26] M. De Hass and J.Th.M. De Hosson, Grain boundary segregation and precipitation in aluminium alloys, *Scripta Mater.*, 44(2001), No. 2, p. 281.
- [27] Y.J. Lang, Y.H. Cai, H. Cui, and J.S. Zhang, Effect of strain-induced precipitation on the low angle grain boundary in AA7050 aluminum alloy, *Mater. Des.*, 32(2011), No. 8-9, p. 4241.